31.1 An Inductor-less Capacitor-less Synchronous Piezoelectric-Electromagnetic Hybrid Energy Harvesting Platform with Coil-Sharing Scheme

Yuchen Wei*[1], Xinling Yue*[1], Zhiyuan Chen[2], Sijun Du[1]

[1]Delft University of Technology, Delft, The Netherlands
[2]Fudan University, Shanghai, China

*Equally Credited Authors (ECAs)

Along with the rise of the Internet of Things (IoT) and edge artificial intelligence (AI), energy harvesting provides a promising sustainable power solution for these edge devices. Piezoelectric (PE) and electromagnetic (EM) transducers are two major ways to harvest ambient vibration energy [1–6]. For PE harvesters, various active rectifiers [7–14] were proposed to improve energy extraction, such as synchronous switch harvesting on inductor (SSHI) rectifiers. However, using high-quality off-chip inductors increases system volumes and costs, while using on-chip (or off-chip) switched capacitors increases chip areas (or system sizes) in addition to a relatively lower overall efficiency. For an EM harvester [15,16], it can be rectified by a boost converter [16] by reusing the EM coil as the inductor. However, off-chip inductors are still required for power conditioning in other DC-DC and regulation stages. Prior works combined these two transducers to harvest more energy from one kinetic source [17]. Unfortunately, all prior structures require additional off-chip inductors or capacitors for different stages, from the rectification to output regulation, as shown in Fig. 31.1.1. It is interesting to think that if the inherent coil of EM harvester can be used for its own boost conversion, why it cannot be used in all other blocks of the whole system, such as PE energy rectification, DC-DC conversion, and output regulations, to eliminate the need for any power components.

In this paper, a hybrid PE-EM energy harvesting platform with a coil-sharing scheme is proposed, as shown in Fig. 31.1.1 bottom, to borrow the active EM coil as a passive inductor for PE bias-flipping, EM energy extraction, DC-DC conversion, and output regulations, without employing any on-chip or off-chip power inductors or capacitors. The proposed energy extraction system provides two regulated outputs, V_{01} (5V) and V_{02} (1.8V), by transferring harvested energy directly to the outputs in one stage without cascading losses. A hybrid harvester was fabricated in-house, shown in Fig. 31.1.1 middle, with a magnet mounted at the free end of a cantilevered PE harvester, and a coil is fixed next to the magnet. When the cantilever vibrates, the PE harvester can be modeled as an AC current source I_P, in parallel a capacitor C_P, and the EM harvester can be modeled as an AC voltage source V_{EM}, in series with the coil's inductance L_{EM} and DC resistance. Due to the synchronous vibration of PE and EM sources, their open-circuit voltages $V_{OC,PE}$ and V_{EM} show a fixed 90° phase difference. The PE energy is extracted by an SSHI rectifier, while the EM energy is rectified via a boost converter (current-mode rectifier) by reusing the EM coil as the inductor. Under light load, the extra harvested energy from both sources will be stored in the battery (BAT). When a heavy load comes, the embedded buck-boost path from the BAT to either C_{01} or C_{02} will be activated to maintain the two outputs, while the coil is shared as a passive DC-DC inductor. At the zero-crossing point (ZCP) of I_P when the PE voltage V_{BF} needs to be flipped, the EM coil is borrowed as a passive SSHI inductor to flip V_{BF}. Thanks to the EM current-mode rectifier, the current in the coil (I_{coil}) is split into multiple phases, and its envelope is in phase with V_{EM}, as shown in Fig. 31.1.1 bot-right. Therefore it makes the ZCP of I_{coil}, V_{EM}, and I_P in-phase, ensuring seamless coil-sharing for PE bias-flipping.

The proposed coil-sharing topology (Fig. 31.1.2 top-left) consists of a negative voltage converter (NVC) and an EM current-mode rectifier for PE and EM sources. The two outputs, V_{01} and V_{02}, are regulated by two 3-threshold hysteresis loops centering at 5V and 1.8V, respectively (Fig. 31.1.2 top-mid). The system has three operation states: source-to-load (S2L), source-to-battery (S2B), and battery-and-source-to-load (BS2L) modes, indicating different energy transfer directions (Fig. 31.1.2 top-right). Take positive cycle EM rectification as an example. Under light load, V_{02} first climbs from V_{REF} to V_{REFH}. The EM rectifier works in S2L mode to sustain V_{02} by the harvested energy. When V_{02} reaches the upper boundary V_{REFH}, it enters the S2B mode to transfer harvested energy to the BAT, leading V_{02} to gradually decrease due to load current. So during light loads, V_{02} is regulated in the upper window formed by V_{REFH} and V_{REF}. When a heavy load comes, EM energy cannot sustain the load, V_{02} will decrease until it reaches the lower boundary V_{REFL}. Then, it triggers the BS2L mode and uses battery power to assist in sustaining the heavy load. After V_{02} is charged back to V_{REF}, the system will enter S2L mode again. So under heavy load, V_{02} is regulated in the lower window formed by V_{REF} and V_{REFL}. Moreover, during BS2L mode, the EM coil still contains harvested energy since the induced voltage V_{EM} still existing; hence, to effectively use the coil as an inductor, its current flow polarity should be same as V_{EM} polarity so that BAT and EM-harvested energy can be transferred together to C_{02}. To achieve this, four embedded power paths are designed in the BS2L mode to charge C_{01} and C_{02} in different V_{EM} polarities with only 2 power switches in a conduction path, as shown in Fig. 31.1.2 bottom.

The proposed system in Fig. 31.1.3 consists of a power stage, an output regulation block, an SSHI controller, and a coil-sharing controller. In the power stage, the NVC-based SSHI block (left) and the coil-sharing switching block (right) are designed to extract energy from PE and EM energy harvesters, respectively. The middle is the modeled hybrid energy harvester. In the output regulation block, dual-output regulation is achieved by two hysteresis window comparators, and the comparators' outputs determine which mode and the power path the system will operate. A maximum voltage selector chooses the higher voltage between V_{BAT} and V_{01} as the system's supply. The SSHI controller controls the synchronous PE voltage bias-flipping. When the rising edge of the CO signal is detected (ZCP of I_P), a bias-flip pulse generator (PG) is triggered to close the two switches S_{BF} to form the LC loop and flip V_{BF}. To avoid the unwanted channel conduction of the NMOS in transmission gate S_{BF} due to the negative spurs, a body-biased driver is designed to adaptively bias the gate by tracking the system's minimum voltage. The coil-sharing controller contains 2 main sub-blocks: the upper EM controller for EM energy harvesting (S2L and S2B mode) and the lower buck-boost controller for using the coil as a DC-DC inductor (BS2L mode). The EM controller is driven by a 1kHz oscillator (OSC) with a reconfigurable duty cycle to perform multi-step current-mode EM rectification, while S_3 and S_4 act as active diodes [19]. The buck-boost controller is activated to enter the BS2L mode during heavy load when the voltage regulation block finds that the harvested energy cannot sustain the two outputs. Then, the controller chooses one of the 4 BS2L power paths to charge V_{01} or V_{02} according to the polarity of V_{EM}. To ensure good energy harvesting performance and proper system operations, the priority of accessing the coil is given to PE bias-flipping, then regulations for C_{02} and C_{01}. However, as shown in Fig. 31.1.3 (top-right), using the coil in the BS2L mode may happen at any time, even crossing two adjacent half-cycles with opposite V_{EM} polarities, and the comparator cannot detect the coil polarity under BS2L mode. However, thanks to the synchronous phases of PE and EM harvesters (explained in Fig. 31.1.1), the PE bias-flip signal can be used as an indicator to reverse the coil polarity to match the reversed V_{EM} polarity. The detailed process for coil direction determination is given in the flow chart in Fig. 31.1.3 bottom-left.

The chip is fabricated in a 0.18μm BCD process, with a 1.08mm² active chip area (Fig. 31.1.7). The hybrid energy harvester was in-house fabricated based on a PE cantilever, a NdFeB magnet, and a hand-winded EM coil with around 2.5mH inductance and 4.5Ω DC resistance. The resonance frequency is 30Hz. Figure 31.1.4 (top-left) shows the PE harvesting, V_{01} regulation (5V with 120mV ripple) and frontend energy harvester waveforms. A 71% PE voltage flipping efficiency is achieved by using the coil to flip. Figure 31.1.4 (top-right) shows the EM harvesting and V_{02} regulation (1.8V with 110mV ripple) waveforms. The I_{coil} signal shows that the coil is always connected in the correct polarity when it is used as an inductor. The spikes in I_{coil} are the moments when the coil is flipping the PE voltage. The spike always happens at the I_{coil} polarity changing point, demonstrating that PE and EM energy sources are strictly orthogonal, exhibiting an exact 90° phase difference. It matches the theoretical waveform in Fig. 31.1.1. The bottom two plots in Fig. 31.1.4 show the regulation of the two outputs under light and heavy load conditions.

Figure 31.1.5 shows the zoomed-in current waveform in the EM coil under heavy load (top left) and its judging algorithm (top right). It verifies that the circuit can track the coil direction under BS2L mode with the PE bias-flip signal as an indicator. The bottom-left figure shows the measured output power of the system, while the x-axis is the open-circuit voltage from the PE harvester, corresponding to the excitation level. The highest extracted power is 2.72mW, and it is dominated by PE and EM energy under low and high excitation levels, respectively. The bottom-right figure shows the measured E2E energy transfer efficiency. The PE-EM combined E2E efficiency peaks at 90%. Figure 31.1.6 compares this work with prior art. This design does not use any on-chip or off-chip passive power component, and hence it achieves a favorable figure of merit (FoM) considering the performance and system volume.

Acknowledgement:
The authors would like to acknowledge Zu-Yao Chang, Lukasz Pakula, and Ron van Puffelen from TU Delft for their technical support. The MPW service and support from TSMC are acknowledged. Corresponding author: Zhiyuan Chen.

2025 IEEE International Solid-State Circuits Conference (ISSCC) | 979-8-3315-4101-9/25/$31.00 ©2025 IEEE | DOI: 10.1109/ISSCC49661.2025.10904574

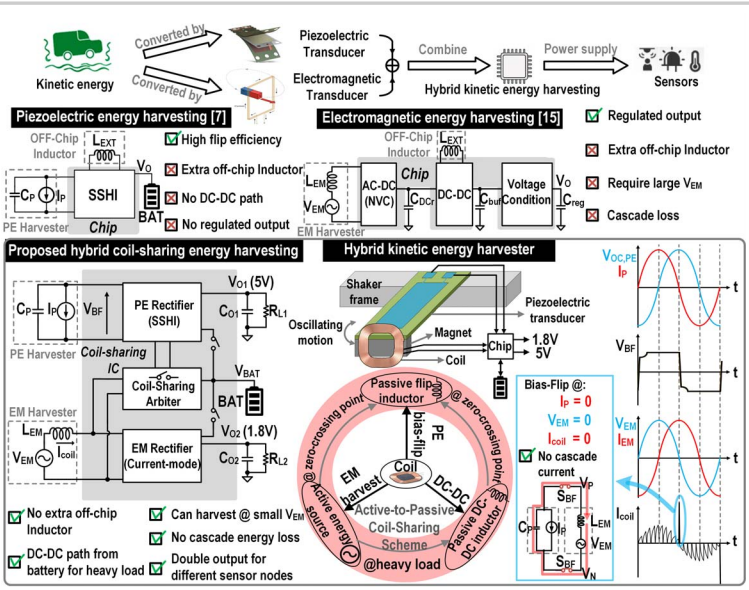

Figure 31.1.1: Proposed synchronous active-to-passive coil-sharing technique and the hybrid energy harvesting platform comparing with previous works.

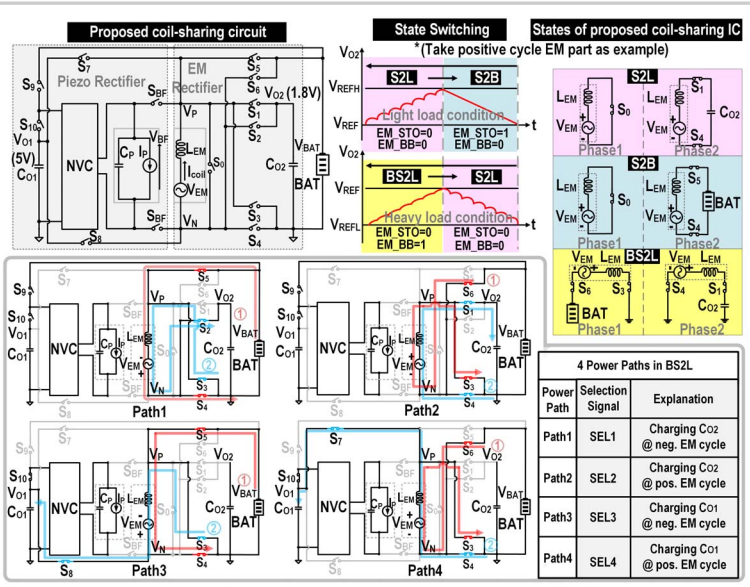

Power Path	Selection Signal	Explanation
Path1	SEL1	Charging C_{O2} @ neg. EM cycle
Path2	SEL2	Charging C_{O2} @ pos. EM cycle
Path3	SEL3	Charging C_{O1} @ neg. EM cycle
Path4	SEL4	Charging C_{O1} @ pos. EM cycle

Figure 31.1.2: Operation states of the proposed system and the four different buck-boost DC-DC paths under BS2L mode (heavy load).

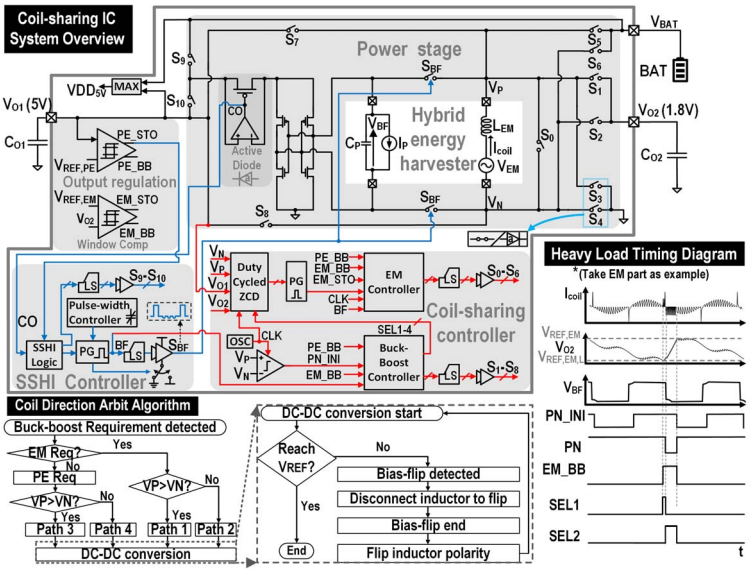

Figure 31.1.3: Proposed coil-sharing circuit details, coil-sharing and direction arbiteration algorithm, and the corresponding waveforms.

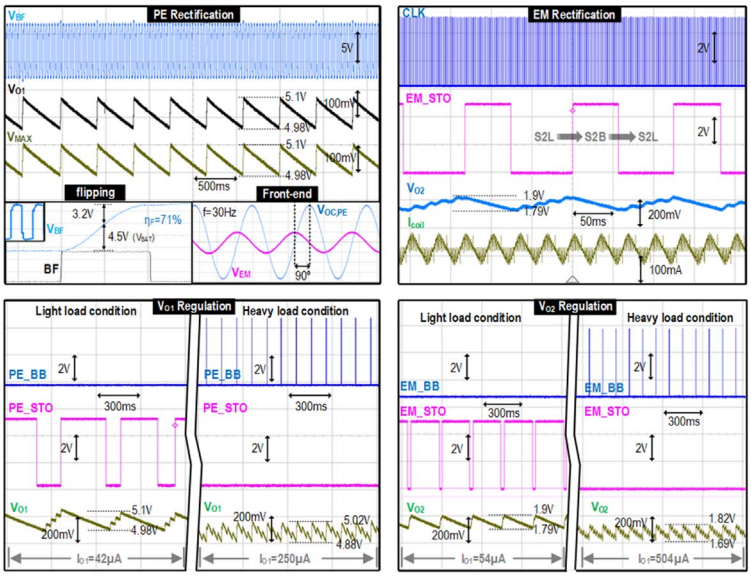

Figure 31.1.4: Measured regular system behavior waveform of PE and EM rectifiers (top); and output regulation with different loads (bottom).

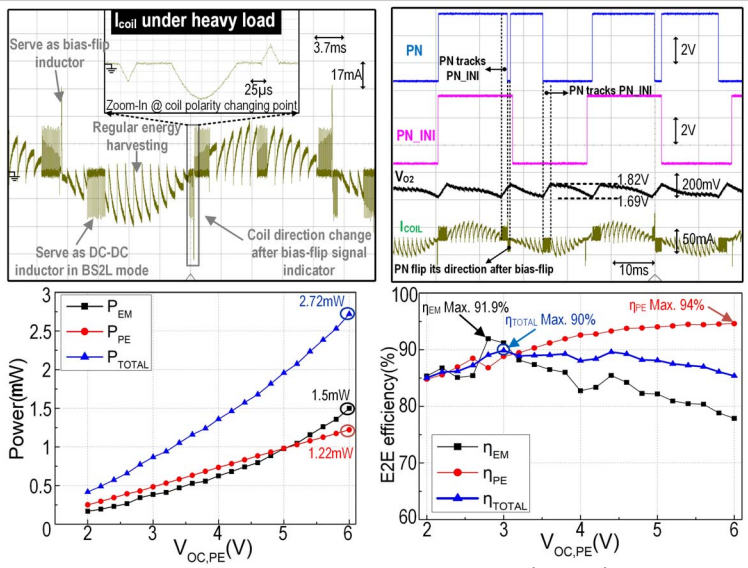

Figure 31.1.5: Measured coil current under heavy load (top left); coil direction judgement algorithm (top right); output power and E2E efficiency versus different $V_{OC,PE}$ (bottom).

Reference	ISSCC'15[15]	TCAS1'19[17]	ISSCC'22[18]	JSSC'23[20]	ISSCC'23[8]	This Work
Process	350nm	180nm	65nm	180nm	180nm	**180nm**
Vibration Harvester	EM	PE+EM	PE/TEG/PV	2*PE/TEG/PV	PE	**PE+EM**
Technique	Conduction Angle	Energy Investment	MSVR SECE	Multi-source Serial Stack	DCB-SSHI	**Coil-Sharing**
Piezoelectric Capacitance	N/A	9n	N/A	100n	42n	**440n**
Operating Freq.	64.4Hz	PE:500Hz EM:20Hz	N/A	25Hz	230Hz	**30Hz**
Cascaded Stage	3	2	1	3	2	**1**
Output Regulation	Yes	No	Yes	No	No	**Yes (1.8V,5V)**
Fully Integrated	No	No	No	No	No	**Yes**
Peak E2E Efficiency	95%	90%(hybrid)	80%(hybrid)	78.8%(hybrid)	N/A	**90%(hybrid)**
Passive Energy Reservoir for Bias-Flip	No Bias-Flip	No Bias-Flip	L=22μH	No Bias-Flip	L=120μH	**None**
Passive Energy Reservoir for DC-DC	L=3.3mH	L=3.3mH	L=22μH	L=470μH	L=120μH	**None**
Normalized V_{NOR}*	34	34	1.22	5.7	2.2	**1**
Max. Output Power	1.2mW	0.1mW	1.2mW	5mW	0.27mW	**2.72mW**
Energy Extraction# Improvement (PE)	N/A	1.48x	3.2x	2.3x	7.38x	**4.7x**
FoM (PE)♦	N/A	0.04	2.48	0.4	3.35	**4.7**

* V_{NOR} = System Volume / Chip Volume
# Energy Extraction Improvement = P_{OUT} / $P_{FBR,MAX}$
♦ FOM = Energy Extraction Improvement / V_{NOR}

Figure 31.1.6: Comparison table of the proposed coil-sharing IC with prior state-of-the-art designs.

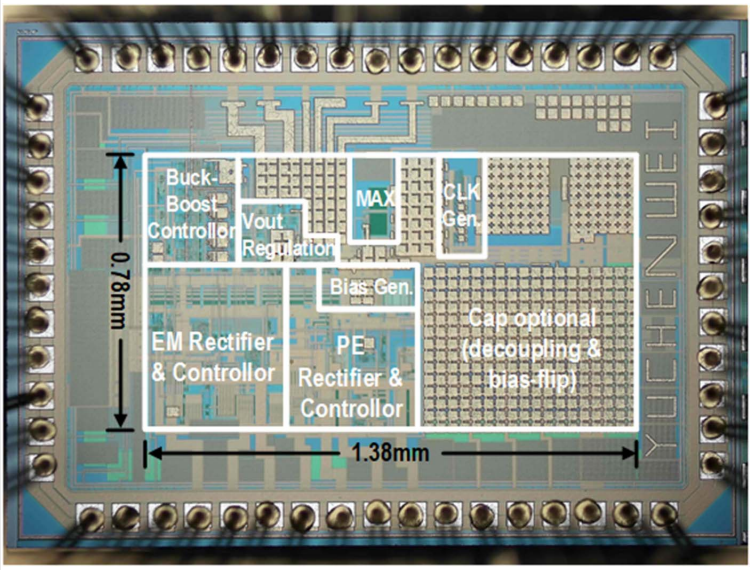

Figure 31.1.7: Chip micrograph.

References:

[1] P.D. Mitcheson et al., "Energy Harvesting From Human and Machine Motion for Wireless Electronic Devices," *Proceedings of the IEEE*, vol. 96, no. 9, pp. 1457-1486, Sept. 2008.

[2] B. H. Calhoun et al., "Design considerations for ultra-low energy wireless microsensor nodes," *IEEE Transactions on Computers*, vol. 54, no. 6, pp. 727-740, June 2005.

[3] M. Gorlatova et al., "Movers and Shakers: Kinetic Energy Harvesting for the Internet of Things," *IEEE Journal on Selected Areas in Communications*, vol. 33, no. 8, pp. 1624-1639, Aug. 2015.

[4] S. Bandyopadhyay and A.P. Chandrakasan, "Platform Architecture for Solar, Thermal, and Vibration Energy Combining With MPPT and Single Inductor," *IEEE JSSC*, vol. 47, no. 9, pp. 2199-2215, Sept. 2012.

[5] P. Mayer et al., "Energy-Positive Activity Recognition - From Kinetic Energy Harvesting to Smart Self-Sustainable Wearable Devices," *IEEE Transactions on Biomedical Circuits and Systems*, vol. 15, no. 5, pp. 926-937, Oct. 2021.

[6] Q. Ju et al., "Power Management for Kinetic Energy Harvesting IoT," *IEEE Sensors Journal*, vol. 18, no. 10, pp. 4336-4345, May 2018.

[7] Y.-W. Jeong et al., Shin, "A Scalable N-Step Equal Split SSHI Piezoelectric Energy Harvesting Circuit Achieving 1170% Power Extraction Improvement and 22nA Quiescent Current with a 1μH-to-10μH Low Q Inductor," *ISSCC*, pp. 438-439, Feb. 2023.

[8] X. Yue et al., "A Bias-Flip Rectifier with a Duty-Cycle-Based MPPT Algorithm for Piezoelectric Energy Harvesting with 98% Peak MPPT Efficiency and 738% Energy-Extraction Enhancement," *ISSCC*, pp. 442-443, Feb. 2023.

[9] Y. K. Ramadass and A. P. Chandrakasan, "An Efficient Piezoelectric Energy Harvesting Interface Circuit Using a Bias-Flip Rectifier and Shared Inductor," *IEEE JSSC*, vol. 45, no. 1, pp. 189-204, Jan. 2010.

[10] J. Lee et al., "A 130V Triboelectric Energy-Harvesting Interface in 0.18 BCD with Scalable Multi-Chip-Stacked Bias-Flip and Daisy-Chained Synchronous Signaling Technique," *ISSC*C, pp. 474-475, Feb. 2022.

[11] A. Morel et al., "Self-Tunable Phase-Shifted SECE Piezoelectric Energy-Harvesting IC with a 30nW MPPT Achieving 446% Energy-Bandwidth Improvement and 94% Efficiency," *ISSCC*, pp. 488-489, Feb. 2020.

[12] A. Quelen et al., "A 30nA Quiescent 80nW-to-14mW Power-Range Shock-Optimized SECE-Based Piezoelectric Harvesting Interface with 420% Harvested-Energy Improvement," *ISSCC*, pp. 150-151, Feb. 2018.

[13] S. Du and A. A. Seshia, "An Inductorless Bias-Flip Rectifier for Piezoelectric Energy Harvesting," *IEEE JSSC*, vol. 52, no. 10, pp. 2746-2757, Oct. 2017.

[14] Z. Chen et al., "A Piezoelectric Energy-Harvesting Interface Using Split-Phase Flipping-Capacitor Rectifier and Capacitor Reuse Multiple-VCR SC DC-DC Achieving 9.3× Energy-Extraction Improvement," *ISSCC*, pp. 424-425, Feb. 2019

[15] J. Leicht et al., "Electromagnetic Vibration Energy Harvester Interface IC with Conduction-Angle-Controlled Maximum-Power-Point Tracking and Harvesting Efficiencies of up to 90%," *ISSCC*, pp. 368-369, 2015.

[16] A. Quelen et al., "Electromagnetic Mechanical Energy-Harvester IC with No Off-Chip Component and One Switching Period MPPT Achieving up to 95.9% End-to-End Efficiency and 460% Energy-Extraction Gain," *ISSCC*, pp. 490-491, Feb. 2020.

[17] S. Chamania et al., "Power-Efficient Hybrid Energy Harvesting System for Harnessing Ambient Vibrations," in *IEEE Transactions on Circuits and Systems I: Regular Papers*, vol. 66, no. 7, pp. 2784-2793, July 2019.

[18] S. Li, et al., "A 32nA Fully Autonomous Multi-Input Single-Inductor Multi-Output Energy-Harvesting and Power-Management Platform with 1.2×105 Dynamic Range, Integrated MPPT, and Multi-Modal Cold Start-Up," *ISSCC*, pp. 472-47, Feb. 2022.

[19] J. Sankman and D. Ma, "A 12-μW to 1.1-mW AIM Piezoelectric Energy Harvester for Time-Varying Vibrations With 450-nA I_0," *IEEE Transactions on Power Electronics*, vol. 30, no. 2, pp. 632-643, Feb. 2015.

[20] X. Wang et al., "Configurable Hybrid Energy Synchronous Extraction Interface With Serial Stack Resonance for Multi-Source Energy Harvesting," *IEEE JSSC*, vol. 58, no. 2, pp. 451-461, Feb. 2023.

979-8-3315-4101-9/25/$31.00 ©2025 IEEE